Atmospheric Research 335 (2026) 108817

Contents lists available at ScienceDirect

Atmospheric Research

journal homepage: www.elsevier.com/locate/atmosres

Impact of tropospheric ozone-radiation interactions on summer ozone air quality over eastern China during 2010–2019

Yuqi Guan [a], Jia Zhu [a,*], Xueqing Wang [b], Lei Chen [a], Xipeng Jin [a], Xu Yue [a], Hong Liao [a,c]

[a] Jiangsu Key Laboratory of Atmospheric Environment Monitoring and Pollution Control, Jiangsu Collaborative Innovation Center of Atmospheric Environment and Equipment Technology, Joint International Research Laboratory of Climate and Environment Change, School of Environmental Science and Engineering, Nanjing University of Information Science and Technology, Nanjing, China
[b] State Key Laboratory of Regional Environment and Sustainability, School of Environment, Tsinghua University, Beijing, China
[c] State Key Laboratory of Climate System Prediction and Risk Management, Nanjing University of Information Science and Technology, Nanjing, China

ARTICLE INFO

Keywords:
Tropospheric ozone
Ozone-radiation interactions
Feedback impacts
Process analysis

ABSTRACT

As an air pollutant and atmospheric oxidant, tropospheric ozone (O_3) is also recognized as a significant greenhouse gas and a key radiatively active species in the atmosphere. In this study, we examine the impact of tropospheric ozone–radiation interactions, explicitly quantifying the effects of meteorological feedback (TrO_3-Met) and photolysis feedback (TrO_3-Phot) on near-surface O_3 concentrations over eastern China in June by using the WRF-Chem model embedded with improved process analysis scheme. A ten-year averaged simulation from 2010 to 2019 is conducted to improve the representativeness of quantified contributions of TrO_3-Met and TrO_3-Phot. Results show that TrO_3-Met increases O_3 concentrations by an average of +0.1 $\mu g \cdot m^{-3}$ over eastern China, with more pronounced effects over the North China Plain (NCP, +0.4 $\mu g \cdot m^{-3}$), the Yangtze River Delta (YRD, +0.5 $\mu g \cdot m^{-3}$), and the Pearl River Delta (PRD +0.1 $\mu g \cdot m^{-3}$), and the enhanced vertical mixing from aloft to the lower level is the dominant process contributing to the elevated O_3 levels. TrO_3-Phot reduces daytime ozone photolysis rate ($J[O^1D]$) by 34.5% and OH radical concentrations by 21.0%, resulting in 1.0% reduction (−1.0 $\mu g \cdot m^{-3}$) in surface O_3 over eastern China, with more substantial reductions over the NCP (−7.8%), YRD (−6.4%), and PRD (−4.2%). The intensified chemical removal process is primarily responsible for the overall decline. Further analysis of O_3-related gas-phase chemical reactions based on integrated reaction rate reveals that weakened HOx-driven oxidation increases the participation of tropospheric O_3 in alternative oxidation pathways, resulting in a negative net O_3 production rate, thereby explaining the reduction in surface O_3 concentrations.

1. Introduction

Tropospheric ozone (O_3) is an important secondary air pollutant formed as a result of photochemical reactions between nitrogen oxides (NO_x) and volatile organic compounds (VOCs), which can significantly affect human health and ecosystems (Sillman, 1999; Cooper et al., 2014; Wang et al., 2017; Lu et al., 2018). Tropospheric O_3 is also a strong oxidant and plays a crucial role in the generation of hydroxyl (OH) radicals. The increase of its concentration will enhance atmospheric oxidizing capacity, promote the formation of secondary pollutants, and consequently lead to a further deterioration in air quality (Feng et al., 2021; Qin et al., 2022). In addition to its roles as an air pollutant and atmospheric oxidant, tropospheric O_3 is a crucial radiation-active gas and the third most significant greenhouse gas in the atmosphere. It absorbs both shortwave and longwave radiation, thereby influencing the atmospheric environment (Myhre et al., 2014).

Tropospheric O_3, acting as a radiation-absorptive gas, can alter Earth's radiation budget, and the changed meteorological fields will induce feedback on near-surface O_3 (Shindell et al., 2006; Chang et al., 2009) (This feedback mechanism is denoted as TrO_3-Met in this study). Du et al. (2023) used the WRF-Chem model to investigate the radiative forcing of tropospheric O_3 on meteorology and air quality over the North China Plain in June 2022. Their results revealed that ozone-radiation interaction caused an increase in air temperature and O_3 concentrations by 0.23 K and 1.2 ppb (1.7%), respectively. Since photolysis rate is closely associated with solar radiation, and tropospheric O_3, as a radiation-active gas, can directly affect photolysis rate by absorbing shortwave radiation. This alteration in photolysis rate can subsequently

* Corresponding author at: Nanjing University of Information Science and Technology, No. 219, Ningliu Road, Nanjing 210044, China.
E-mail address: jiazhu@nuist.edu.cn (J. Zhu).

https://doi.org/10.1016/j.atmosres.2026.108817
Received 18 November 2025; Received in revised form 21 January 2026; Accepted 29 January 2026
Available online 30 January 2026

lead to feedback impacts on O_3 concentrations (He and Carmichael, 1999) (This feedback mechanism is denoted as TrO_3-Phot in this study). Yang et al. (2025) applied XGBoost model coupled with an interpretable SHAP algorithm to investigate the influence of photolysis rates on O_3 concentration during non-rainy days in Qingdao in 2023. They found that O_3 photolysis rate (i.e., $J[O^1D]$) exhibits a negative correlation with O_3 concentration, and is the fifth most significant factor affecting summer O_3.

When examining the influence of interactions between atmospheric pollutants and radiation, there are currently limited studies that quantify the impact of the interaction between tropospheric O_3 and radiation. Existing studies predominantly focus on the radiative effects associated with aerosols (Wang et al., 2016; Xing et al., 2017; Gao et al., 2020; Yang et al., 2021). Qu et al. (2020) used the UKESM1 model and found that aerosol–radiation feedback could reduce surface shortwave radiation, leading to a lower planetary boundary layer height (PBLH) and decreased surface wind speed, thereby reducing annual mean surface O_3 by 3.84 ppb (14.9%) over the North China Plain during 2014. Li et al. (2025) conducted simulations by WRF-Chem to show that aerosol-radiation interactions reduced surface ozone by 2.69 ppb through lowering surface temperature and PBLH in the Yangtze River Delta in January 2020. Some studies have analyzed the impact of TrO_3-Met but mainly focused on its effects on meteorology, without further exploring the feedback influence on O_3 concentrations (Shindell et al., 2006; Chang et al., 2009; Li et al., 2018). Xie et al. (2016) used BCC_AGCM2.0.1_CUACE/Aero model to quantify the influence of tropospheric O_3 radiative forcing on meteorological fields, and found that the increase in concentrations of tropospheric O_3 from 1850 to 2013 could produce a positive effective radiative forcing of +0.46 W m^{-2} which further led to a global increase in surface temperature by 0.36 K and precipitation by 0.02 mm, respectively. Only a few studies have quantified the impact of TrO_3-Met on O_3 concentrations (Taha and Sailor, 2010; Du et al., 2023). Taha and Sailor (2010) applied a two-way coupled MM5-CMAQ model to simulate an O_3 pollution episode in the US in July 1998, and reported that TrO_3-Met could increase the peak O_3 concentrations by 2–4 ppb. Zhou. (2010) conducted WRF-Chem to analyze the interactions between tropospheric O_3 and radiation over East Asia during 23–24 June in 2009, and pointed out that TrO_3-Met increased surface O_3 by 0.43 ppb, with a maximum increase of 0.71 ppb. However, these previous studies on the impact of TrO_3-Met on near-surface O_3 have been limited to quantitative analyses of individual cases (e.g., short-term ozone pollution episodes) and thus lack the statistical robustness needed to derive representative conclusions. Meanwhile, from the perspective of radiation-active gas, quantitative investigation into the impact of tropospheric O_3 on photolysis rates through the absorption of shortwave radiation—and the subsequent feedback on O_3 concentration, referred to as TrO_3-Phot—has not yet yielded significant results.

Therefore, this study aims to systematically quantify the impacts of TrO_3-Met and TrO_3-Phot on concentrations of near-surface O_3 by using the fully coupled online Weather Research and Forecasting with Chemistry (WRF-Chem) model over eastern China in June during 2010–2019. The ten-year averaged simulation result can enhance the representativeness of quantified contributions of TrO_3-Met and TrO_3-Phot to some extent. Additionally, the improved integrated process rate (IPR) and integrated reaction rate (IRR) are also applied to identify the dominant physical and/or chemical process responsible for the impacts of TrO_3-Met and TrO_3-Phot. This paper is organized as follows: in Section 2, we describe observational data, model configuration, numerical experiments, and process analysis. Model evaluation is provided in Section 3. Results and discussions are presented in Section 4. Conclusions and limitations are provided in Section 5.

2. Data and methods

2.1. Tropospheric column ozone from satellite measures

The spatio-temporal evolution characteristics of global tropospheric column ozone (TrCO) concentration are first analyzed to identify hotspots for further quantifying the impacts of TrO_3-Met and TrO_3-Phot through model simulations. Retrieved TrCO from OMI/MLS, OMPS/MERRA2, and EPIC/MERRA are selected (https://acd-ext.gsfc.nasa.gov/Data_services/cloud_slice/), including multi-CMIP6-model simulations (MOHC-UKESM1, NOAA-GFDL-ESM4, MIROC-ES2H, MRI-ESM2, IPSL-CM5A2-INCA, IPSL-CM6A-LR-INCA, GISS-E2, https://aims2.llnl.gov/search/cmip6/). By analyzing the multi-year mean (Fig. 1) and multi-year trend (Table 1) of TrCO, it can be concluded that the concentration of TrCO in eastern China is the highest among regions at the same latitude worldwide, with values of 38.3 DU from OMI/MLS, 37.6 DU from OMPS/MERRA2, 40.6 DU from EPIC/MERRA, and 42.1 DU from CMIP6, and exhibits a significant increasing trend of +2.6 DU/decade, +0.0 DU/decade, +0.5 DU/decade, and + 1.7 DU/decade, respectively. Therefore, eastern China is selected as the final target region for model simulation, as shown in Fig. S1.

2.2. Meteorology and air pollutants from monitoring observations

To evaluate the simulation performance of the WRF-Chem model, this study utilizes in-situ observations of 2 m temperature (T_2), 2 m relative humidity (RH_2), and 10 m wind speed (WS_{10}) obtained from the University of Wyoming (http://weather.uwyo.edu/). Ground-level O_3 concentrations are sourced from the China National Environmental Monitoring Centre (CNEMC, https://air.cnemc.cn:18007).

2.3. Model configuration

The online coupled Weather Research and Forecasting with Chemistry (WRF-Chem v4.2.2) model (Grell et al., 2005; Fast et al., 2006) is used in this study to quantitatively explore the impacts of interactions between tropospheric O_3 and radiation (including TrO_3-Met and TrO_3-Phot) on near-surface O_3 over eastern China. Fig. S1 shows the simulation domain that covers most regions of eastern China with a horizontal resolution of 27 km and grid points of 71 (west–east) × 92 (south–north). The model contains 60 vertical levels from the surface to the top of 100 Pa.

The meteorological initial and lateral boundary conditions are provided by the fifth generation of European Centre for Medium-Range Weather Forecasts (ECMWF) atmospheric reanalysis (ERA5, https://cds.climate.copernicus.eu/datasets), with the spatial resolution of 0.25° and temporal resolution of 3-h. The chemical initial and boundary conditions are provided by the Community Atmosphere Model with Chemistry (CAM-Chem, https://www.acom.ucar.edu/cam-chem/cam-chem.shtml), featuring a spatial resolution of 1° × 1.25° and a temporal resolution of 6-h.

MOZART (the model for ozone and related chemical tracers) is selected as the gas-phase chemical mechanism (Brasseur et al., 1998), and the full eight-bin MOSAIC (Model for Simulating Aerosol Interactions and Chemistry) module with aqueous chemistry is used to simulate aerosol evolution (Zaveri et al., 2008). The photolysis rates are calculated by the new TUV (Tropospheric Ultraviolet and Visible) scheme modified by NCAR (https://www2.acom.ucar.edu/modeling/tropospheric-ultraviolet-and-visible-tuv-radiation-model) (Madronich and Flocke, 1997). The rapid radiative transfer model for general circulation models (RRTMG) is used to treat both shortwave and longwave radiation in the atmosphere (Iacono et al., 2008). Other major parameterizations used in this study are listed in Table S1.

Anthropogenic emissions are taken from the Multi-resolution Emission Inventory for China (MEIC, http://www.meicmodel.org/) (Li et al., 2017). The inventory provides emissions of sulfur dioxide (SO_2),

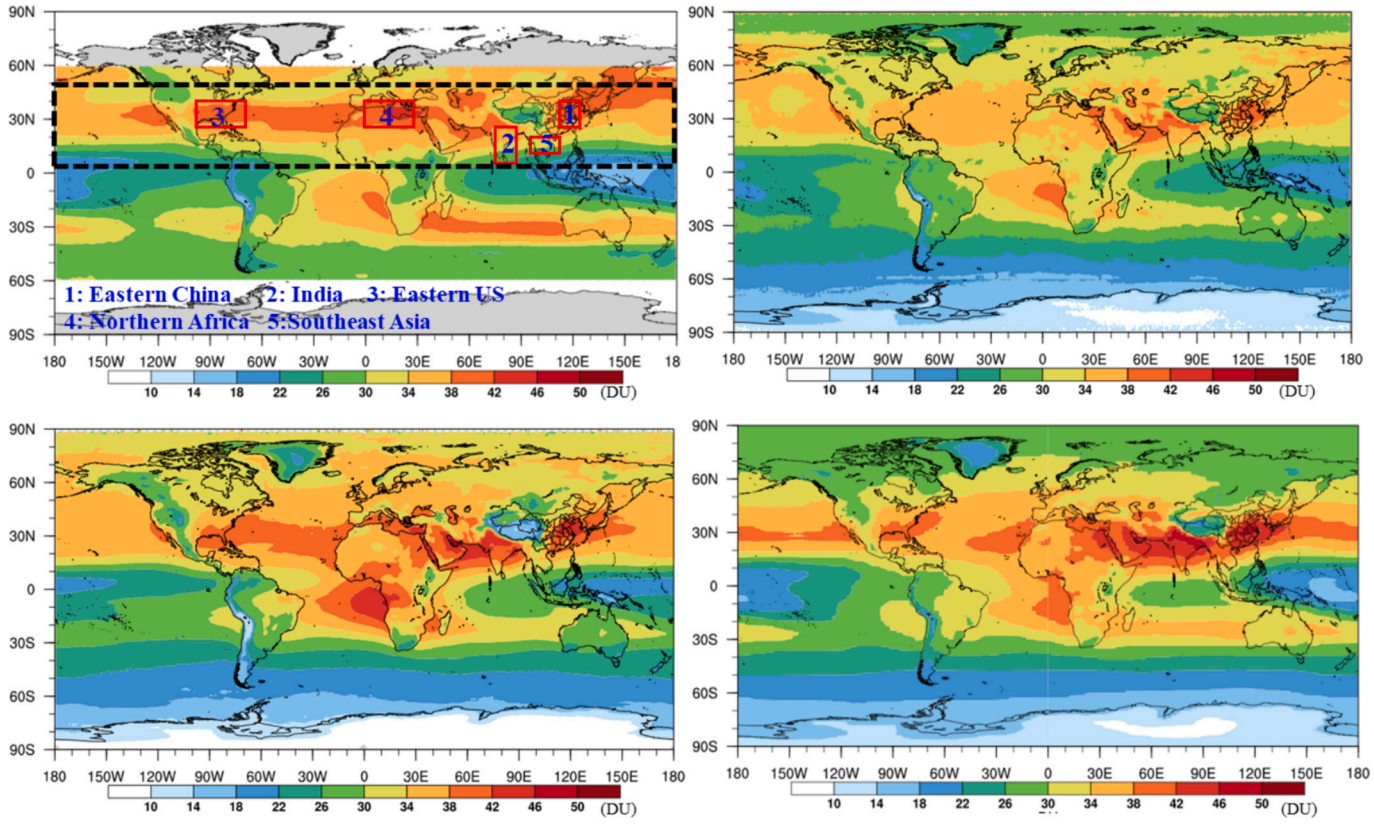

Fig. 1. Spatial distribution of global tropospheric column ozone (TrCO) retrieved from (a) OMI/MLS during 2005–2020, (b) OMPS/MERRA2 during 2012–2022, (c) EPIC/MERRA during 2015–2022, and (d) multi-model simulation results of CMIP6 during 2005–2014 in June. Red boxes in (a) represent the five hotspots (Eastern China, India, Eastern US, Northern Africa, and Southeast Asia) with high TrCO concentrations over the Northern Hemisphere. (For interpretation of the references to colour in this figure legend, the reader is referred to the web version of this article.)

Table 1
Multi-year mean (multi-year trend) of tropospheric column ozone retrieved from OMI/MLS, OMPS/MERRA2, EPIC/MERRA, and CMIP6 simulations in June averaged over regions of Eastern China, India, Eastern US, Northern Africa, and Southeast Asia with unit of DU (DU decade^{-1}).

Region	OMI/MLS (2005–2020)	OMPS/MERRA2 (2012−2022)	EPIC/MERRA (2015–2022)	CMIP6 (2005–2014)
Eastern China	38.3 (+2.6)	37.6 (0.0)	40.6 (+0.5)	42.1 (+1.7)
India	33.5 (+2.2)	34.6 (+0.9)	38.7 (+1.1)	41.0 (+2.3)
Eastern US	37.5 (+1.2)	34.9 (+0.8)	37.8 (+0.1)	37.1(+0.3)
Northern Africa	39.5 (+1.7)	35.1 (+1.4)	37.9 (−1.5)	37.5 (+0.5)
Southeast Asia	30.8 (+3.2)	31.7 (−0.2)	34.2 (+1.0)	36.8 (+1.7)

nitrogen oxides (NOx), carbon monoxide (CO), non-methane volatile organic compounds (NMVOCs), ammonia (NH_3), black carbon (BC), organic carbon (OC), primary PM_{10} (particulate matter with an aerodynamic diameter of 10 μm and less), and primary $PM_{2.5}$. Biogenic emissions are calculated online by the Model of Emissions of Gases and Aerosols from Nature (MEGAN) (Guenther et al., 2006). Biomass-burning emissions are obtained from Fire INventory from NCAR (FINN) (Wiedinmyer et al., 2011).

2.4. Sensitivity experiments

In order to quantify the impacts of TrO_3-Met and TrO_3-Phot on near-surface O_3 concentrations, three sensitivity experiments have been designed (Table 2). (1) BASE: the base simulation is coupled with the interactions between tropospheric O_3 and radiation, including both impacts of TrO_3-Met and TrO_3-Phot; (2) $WoTrO_3$Met: same as BASE, but the impact of TrO_3-Met is turned off (tropospheric ozone concentration is set to be a very small value in the RRTMG shortwave and longwave radiation modules); (3) $WoTrO_3$Phot: same as BASE, but the impact of TrO_3-Phot is turned off (optical depth due to ozone absorption is set to be a very small value in the TUV photolysis module). All the experiments are conducted from 27 May to 30 June, with the first 5 days as the model spin-up, and a ten-year simulation from 2010 to 2019 is conducted, which, to some extent, can enhance the representativeness of quantified contributions of TrO_3-Met and TrO_3-Phot. Simulation results from the BASE case are used to compare with observations for evaluating the model performance. The differences between BASE and $WoTrO_3$Met ($WoTrO_3$Phot) represent the impacts of TrO_3-Met (TrO_3-Phot).

Table 2
Descriptions of model sensitivity experiments.

Experiment	Impact of TrO_3-Met	Impact of TrO_3-Phot
BASE	on	on
$WoTrO_3$Met	off	on
$WoTrO_3$Phot	on	off

2.5. Process analysis

Process analysis module can quantify the contribution of individual physical/chemical process to model predictions and display the relative importance of each process. The module can be divided into two parts: Integrated Process Rate (IPR) analysis and Integrated Reaction Rate (IRR) analysis.

Traditional IPR analysis can only be used to assess the contribution of different processes to ozone variation between two time points (Li et al., 2018; Zhang et al., 2024; Qiao et al., 2024). In this study, we apply the improved IPR, which can quantify the impact of each process on the mean concentration averaged over any time period. More details about the improved IPR can be found in Chen et al. (2023). Four major physical/chemical processes, including advection (TRAN), vertical mixing (VMIX), sub-grid convection (SGCV), and gas-phase chemistry (GASC), are calculated in the improved IPR.

The IRR analysis can be used to compare the rates of gas-phase chemical reactions (Kitayama et al., 2019; Chuang et al., 2024). According to ozone-related chemical generation (consumption) rates diagnosed from IRR, we can elucidate the underlying mechanism of increased/decreased near-surface ozone due to the impacts of TrO_3-Met and TrO_3-Phot.

3. Model evaluation

Reliable simulation of meteorological variables and air pollutant concentrations by the WRF-Chem model serves as the foundation for quantifying the impacts of interactions between tropospheric O_3 and radiation on near-surface ozone. This section presents a detailed comparison between simulation results of BASE in June during 2010–2019 and the corresponding observations including meteorological fields (2010–2019), near-surface O_3 concentrations (2013–2019), and TrCO concentrations (2010–2019).

3.1. Model evaluation for meteorological variables and near-surface ozone concentrations

Fig. 2 shows the spatio-temporal variations in observed and simulated 2-m temperature (T_2), 2-m relative humidity (RH_2), 10-m wind speed (WS_{10}), and maximum daily 8-h average (MDA8) O_3 concentrations averaged over eastern China in June during 2010–2019. As shown in Fig. 2(a1-a2) (b1-b2), WRF-Chem model can reproduce the spatial distribution and temporal evolution of observed T_2 (RH_2) with normalized mean bias (NMB) of −3.3% (+3.7%), root mean square error (RMSE) of 1.3 °C (3.7%), index of agreement (IOA) of 0.92 (0.93), and correlation coefficient (R) of 0.91 (0.87), respectively. WRF-Chem overestimates WS_{10} (Fig. 2(c1-c2)), with NMB of +12.7%, which may be caused by the unresolved topographical features (Jiménez and Dudhia, 2012). The positive bias in wind speed can also be found in many other studies (Gao et al., 2015; Qiu et al., 2017). As demonstrated in Fig. 2(d2), WRF-Chem reproduces the spatial distribution of observed MDA8 O_3 reasonably well, with high values over large city clusters. The RMSE is 36.1 $\mu g \cdot m^{-3}$ and IOA is 0.59. The model can also depict the temporal variations in MDA8 O_3 fairly well (Fig. 2(d1)), with NMB of 10.0% and R of 0.76, respectively.

3.2. Model evaluation for tropospheric column ozone concentrations

This study aims to investigate the impact of interactions between tropospheric O_3 and radiation. Therefore, we further validate the simulated TrCO with observations retrieved from the OMI-MLS satellite. From Fig. 3 we can find that the simulated spatial pattern of TrCO is

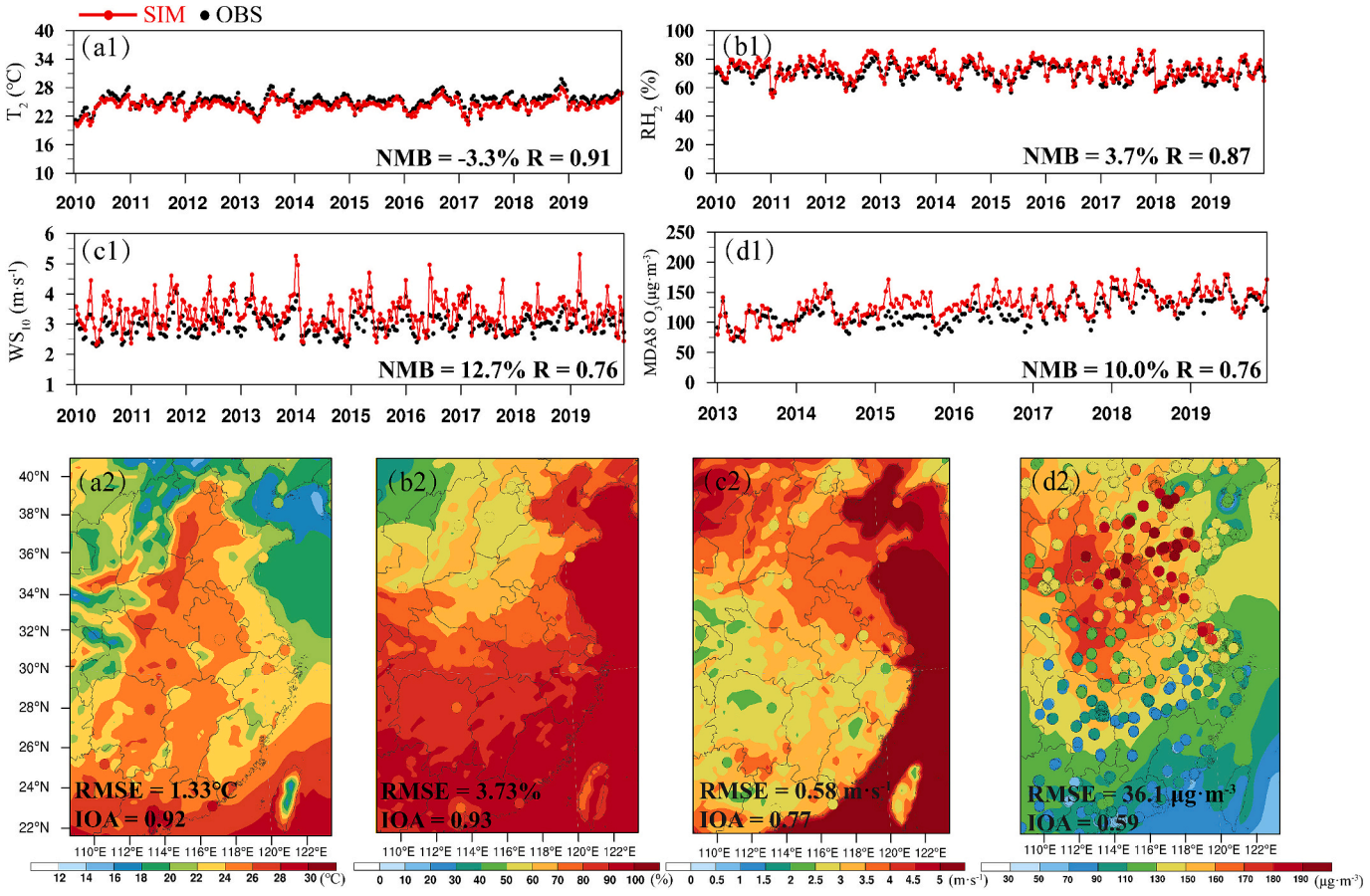

Fig. 2. (a1-d1) Time series of observed (black dots) and simulated (red dotted lines) daily 2-m temperature (T_2), 2-m relative humidity (RH_2), 10-m wind speed (WS_{10}), and MDA8 O_3 concentrations in June during 2010–2019 averaged over all observation sites in eastern China. (a2–d2) Spatial distributions of observed (circle) and simulated (colored) 10-year-mean T_2, RH_2, WS_{10}, and MDA8 O_3 averaged in June over eastern China. Statistics of root mean square error (RMSE), index of agreement (IOA), normalized mean bias (NMB), and correlation coefficient (R) are shown at the bottom of each panel.

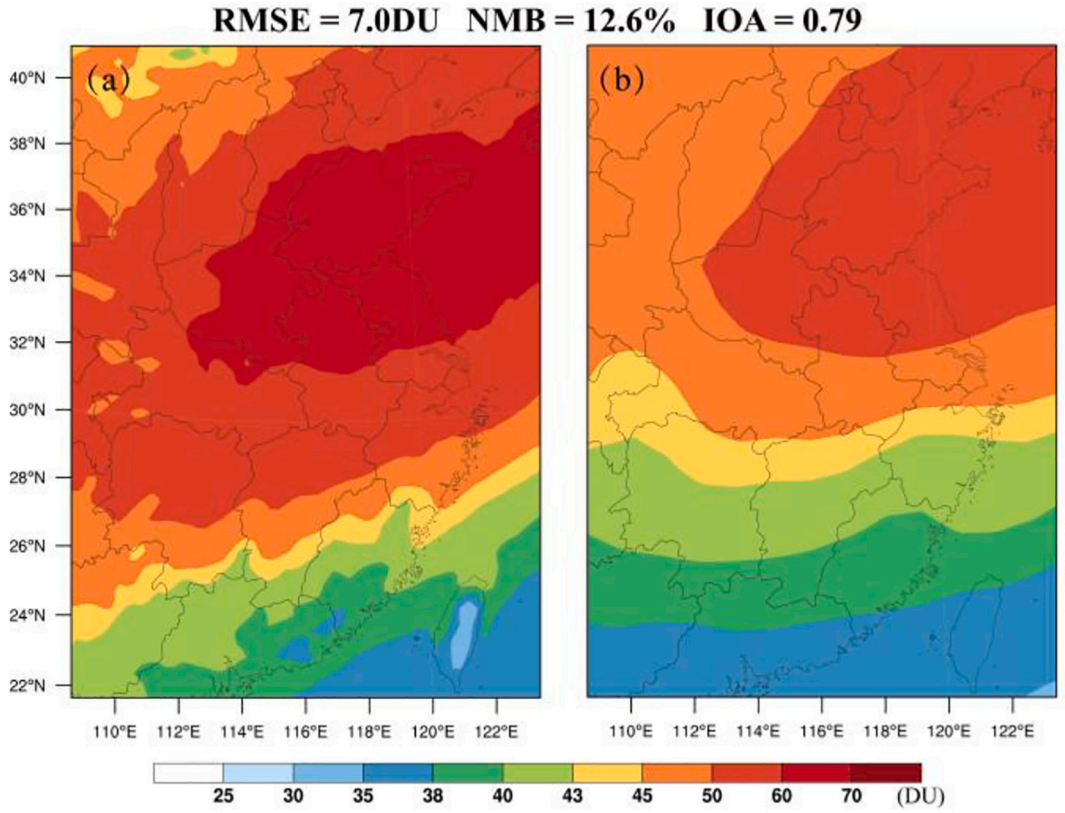

Fig. 3. Spatial distribution of (a) simulated tropospheric column ozone (TrCO) concentration and (b) satellite retrieved TrCO derived from OMI-MLS averaged in June during 2010–2019 over eastern China. Statistics of root mean square error (RMSE), normalized mean bias (NMB), and index of agreement (IOA) are shown at the top.

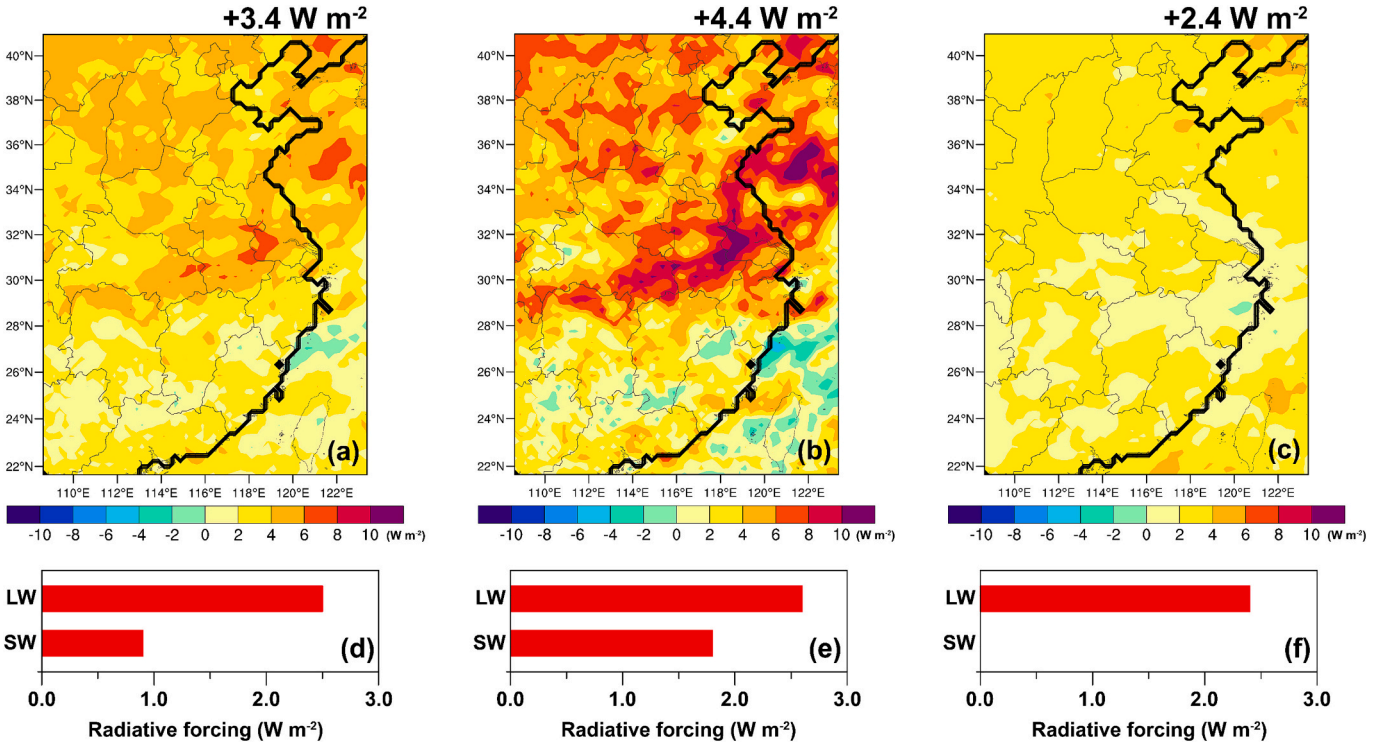

Fig. 4. Spatial distribution of the differences in simulated daily (left), daytime (07:00–18:00 LST, middle), and nighttime (19:00–6:00 LST, right) (a-c) all-sky net radiative forcing at the tropopause between BASE and WoTrO$_3$Met cases (BASE minus WoTrO$_3$Met) averaged in June during 2010–2019, and (d-f) the contributions of shortwave (SW) and longwave (LW) radiative fluxes. Regional mean changes averaged over eastern China are shown at the top to each panel.

consistent with satellite data with the NMB of 12.6% and IOA of 0.79. In general, the model can well reproduce the features of observed meteorology and tropospheric O_3 over eastern China.

4. Results and discussions

4.1. Impacts of tropospheric ozone as a radiation-absorptive gas on meteorology

Fig. 4 illustrates the impact of tropospheric O_3 acting as a radiation-absorptive gas on the net radiative forcing at the tropopause. As shown in Fig. 4, TrO_3-Met increases the daily, daytime, and nighttime tropospheric net radiative forcing by +3.4, +4.4, and + 2.4 W m^{-2}, respectively. The daytime changes are more pronounced compared to that at nighttime. Fig. 4(d-f) further decompose the impact of TrO_3-Met on longwave and shortwave radiative fluxes. TrO_3-Met increases the daily, daytime, and nighttime longwave (shortwave) radiative fluxes by +2.5 (+0.9), +2.6 (+1.8), and +2.4 (+0.0) W m^{-2} averaged over eastern China, respectively. The variation of longwave radiation dominates the overall impact, reflecting the greenhouse gas properties of tropospheric O_3.

The alteration of radiation balance by TrO_3-Met will further affect meteorological variables. As shown in Fig. 5(a), TrO_3-Met leads to an increase in air temperature by +0.05 °C over eastern China due to the change of radiative fluxes, with a maximum change of +0.12 °C. Regions experiencing temperature increases align closely with areas of enhanced net radiative forcing (Fig. 4a). Fig. 5(c) illustrates the impact of TrO_3-Met on PBLH, revealing that the regions of elevated PBLH generally coincide with the warming zones, with a regional mean increase of 1.9 m over eastern China. The changes in certain areas of the middle and lower reaches of the Yellow River and the Yangtze River Delta are more pronounced, with a local maximum change of +21.8 m. This spatial heterogeneity may be attributed to the influence of temperature changes on vertical turbulent motion or the variations in BOT_SW perturb near-surface energy fluxes, thereby modulating convective intensity and altering PBLH. A similar phenomenon was also reported by Yang et al. (2021). TrO_3-Met reduces the near-surface relative humidity, with a relatively small regional mean of −0.11% (Fig. 5b), which may be ascribed to the influence of temperature changes. This phenomenon is consistent with the study of Pierrehumbert et al. (2007).

4.2. Feedback impacts of tropospheric ozone as a radiation-absorptive gas on ozone

The changed tropospheric radiation budget and meteorological variables due to TrO_3-Met will induce feedback impacts on near-surface ozone. Fig. 6(a) presents the changes in near-surface O_3 concentrations over eastern China after considering the influence of TrO_3-Met. TrO_3-Met can increase the daily ozone concentrations by +0.1 μg·m^{-3}, with a maximum change of +1.2 μg·m^{-3}. This increase is particularly pronounced in major metropolitan regions, such as the North China Plain (NCP, +0.4 μg·m^{-3}), Yangtze River Delta (YRD, +0.5 μg·m^{-3}), and Pearl River Delta (PRD, +0.1 μg·m^{-3}).

To explain the underlying mechanism of the impact of TrO_3-Met on ozone concentrations, we quantify the contributions of different physical and chemical processes to monthly ozone by using the improved IPR analysis, and discuss the difference between cases of BASE and $WoTrO_3$Met. Fig. 6(b) indicates that when the impact of TrO_3-Met is considered, the weakened advection (TRAN) input and the enhanced gas-phase chemical (GASC) removal both decrease the concentration of near-surface O_3 by 4.1 and 3.5 μg·m^{-3} averaged over eastern China, respectively. While, the changed sub-grid convection (SGCV) and vertical mixing (VMIX) both increase the O_3 concentrations by +1.2 and + 6.5 μg·m^{-3}, respectively, and the VMIX process dominates the final change of O_3 (+0.1 μg·m^{-3}) over eastern China. Similar process contributions can also be quantified over NCP, YRD, and PRD (Fig. 6(c-e)). For instance, TrO_3-Met decreases the contributions of GASC (−10.8 μg·m^{-3} for NCP, −33.8 μg·m^{-3} for YRD, and − 24.8 μg·m^{-3} for PRD) and TRAN (−5.6 μg·m^{-3} for NCP, −8.6 μg·m^{-3} for YRD, except for PRD with a positive contribution of +3.9 μg·m^{-3}), but enhances the contributions of SGCV (+4.8 μg·m^{-3} for NCP, +3.0 μg·m^{-3} for YRD, and + 9.2 μg·m^{-3} for PRD) and VMIX (+12.0 μg·m^{-3} for NCP, +39.9 μg·m^{-3} for YRD, and + 11.8 μg·m^{-3} for PRD).

4.3. Impacts of tropospheric ozone as a radiation-active gas on photolysis rate

As a radiation-active gas, tropospheric ozone can also affect gas-

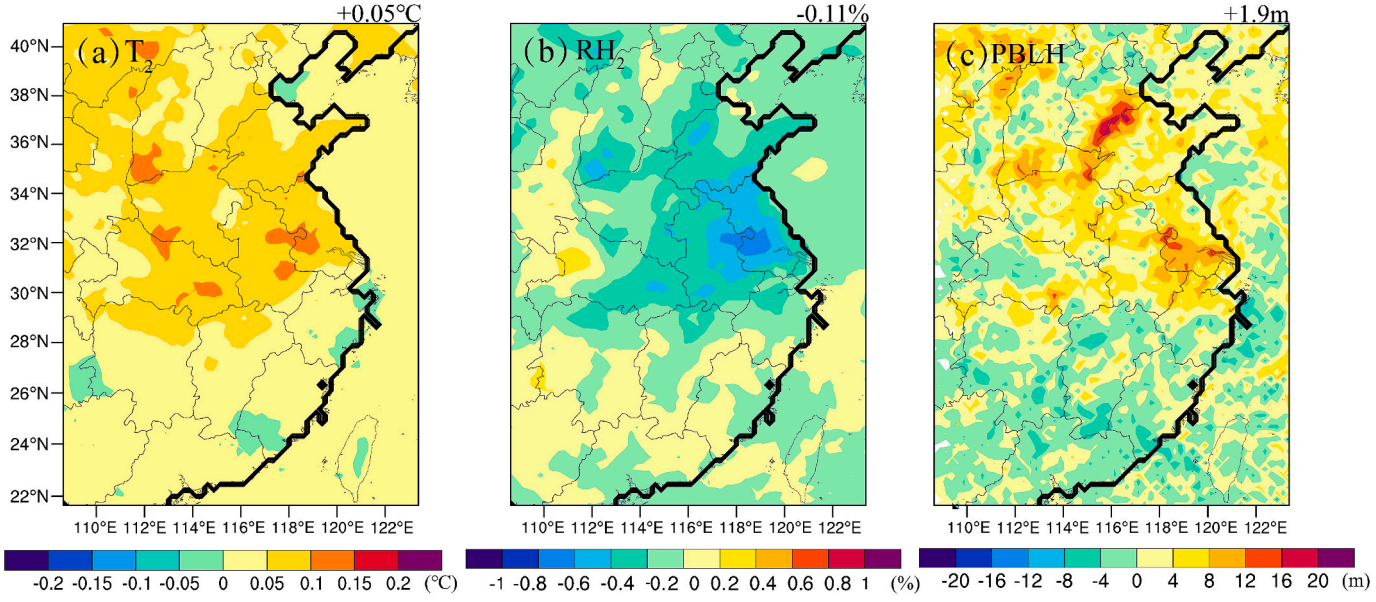

Fig. 5. Spatial distribution of the differences in simulated daily (a) near-surface temperature (T_2), (b) near-surface relative humidity (RH_2), and (c) planetary boundary layer height (PBLH) between the cases of BASE and $WoTrO_3$Met (BASE minus $WoTrO_3$Met) averaged in June during 2010–2019. Regional mean changes averaged over eastern China are shown at the top to each panel.

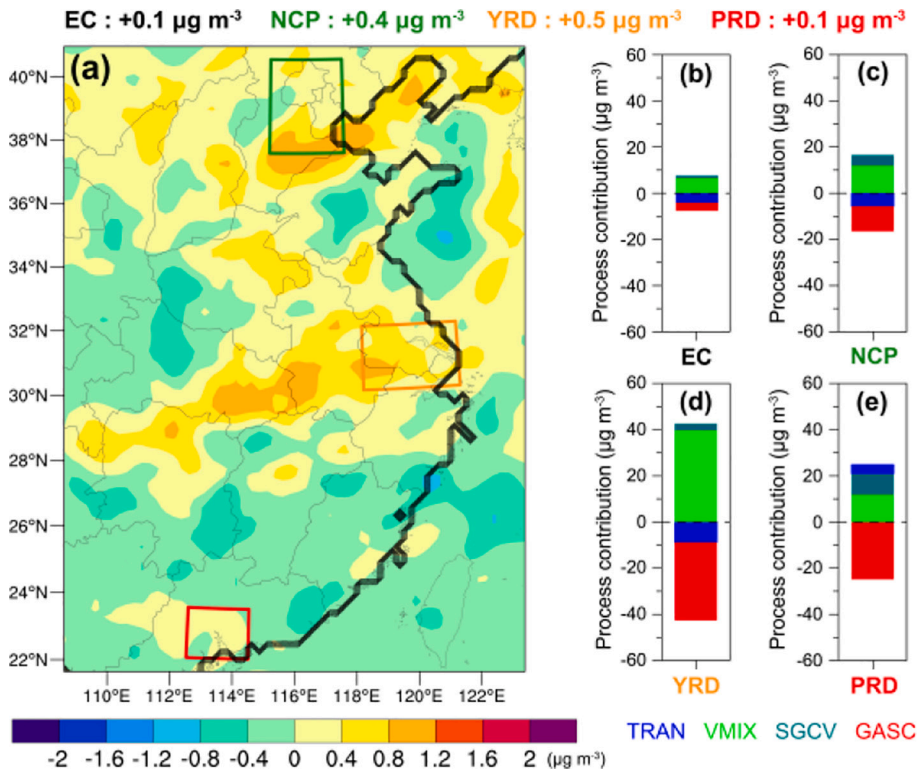

Fig. 6. (a) Spatial distribution of the difference in simulated daily near-surface ozone between the cases of BASE and WoTrO$_3$Met (BASE minus WoTrO$_3$Met) averaged in June during 2010–2019. Process contributions of TRAN (advection), VMIX (vertical mixing), SGCV (sub-grid convection), and GASC (gas-phase chemistry) to ozone changes averaged over (b) eastern China (EC), (c) North China Plain (NCP), (d) Yangtze River Delta (YRD), and (e) Pearl River Delta (PRD) are also shown.

phase photolysis due to the optical depth of ozone molecular absorption. In order to quantify the impact of TrO$_3$-Phot on ozone air quality, the changes in photolysis rate of $J[O^1D]$, $J[NO_2]$, and $J[O^3P]$ are first analyzed. As shown in Fig. 7(a), TrO$_3$-Phot causes a significant decrease in daytime $J[O^1D]$ with a regional mean of −34.5% (-0.7×10^{-5} s^{-1}) over eastern China. The changes over regions with large TrCO (such as NCP and YRD) are more significant, with values of −40.4% for NCP and − 37.9% for YRD, respectively. The impacts of TrO$_3$-Phot on $J[NO_2]$ and $J[O^3P]$ are relatively small (Fig. S2), with the reductions of 0.4% and 2.0% averaged over eastern China.

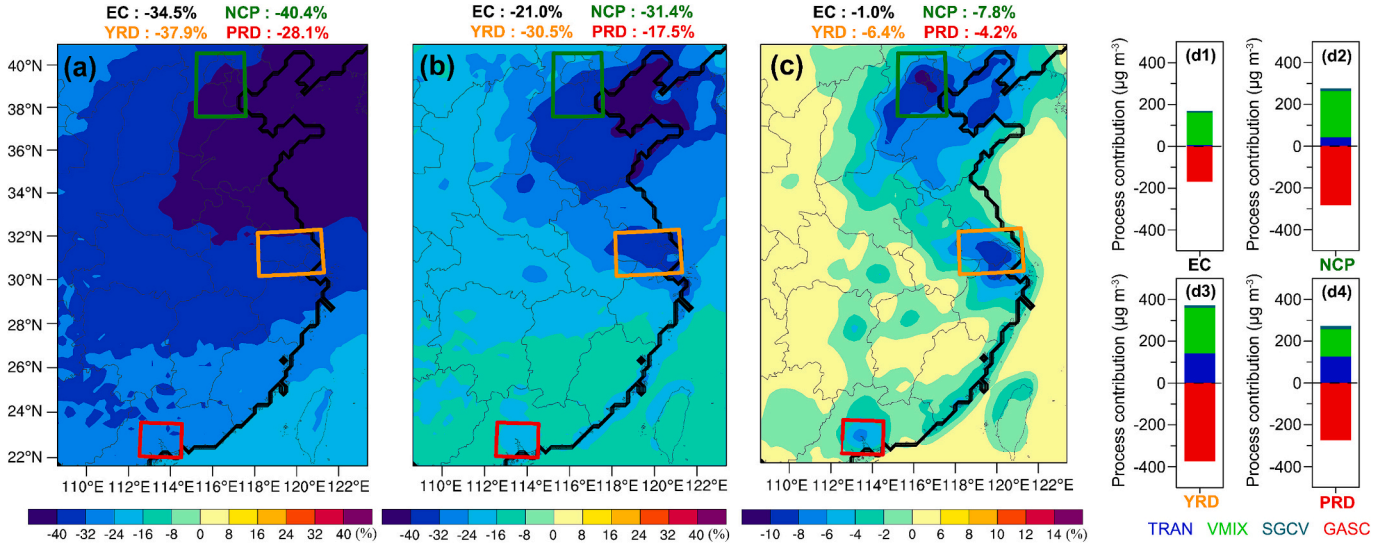

Fig. 7. Spatial distribution of relative changes in simulated daytime (07:00–18:00 LST) (a) photolysis rate of ozone ($J[O^1D]$), (b) hydroxyl radical (OH), and (c) near-surface ozone between the cases of BASE and WoTrO$_3$Phot (BASE minus WoTrO$_3$Phot) averaged in June during 2010–2019. Process contributions of TRAN (advection), VMIX (vertical mixing), SGCV (sub-grid convection), and GASC (gas-phase chemistry) to ozone changes averaged over (d1) eastern China (EC), (d2) North China Plain (NCP), (d3) Yangtze River Delta (YRD), and (d4) Pearl River Delta (PRD) are also shown.

4.4. Feedback impacts of tropospheric ozone as a radiation-active gas on ozone

In the troposphere, the concentration of OH radical is closely related to the photolysis rate of ozone ($J[O^1D]$), and the decrease in $J[O^1D]$ due to TrO_3-Phot will further reduce daytime OH. Fig. 7(b) exhibits that OH radical concentration is decreased by 21% (-1.3×10^6 mol cm^{-3}) over eastern China with more pronounced reductions over NCP (−31.4%) and YRD (−30.5%).

Decreased $J[O^1D]$ and OH radicals will further affect O_3 concentrations. Fig. 7(c) shows the spatial distribution of changed daytime near-surface O_3 due to TrO_3-Phot. TrO_3-Phot reduces O_3 concentrations by 1.0% (-1.0 μg·m^{-3}) averaged over eastern China, with areas exhibiting significant decreases (e.g., −7.8% in NCP, −6.4% in YRD, and − 4.2% in PRD) closely corresponding to those showing diminished OH radical concentrations. This reduction is likely attributable to a weakened free radical cycling process, which may in turn affect ozone-related chemical reactions.

To explain the underlying mechanism of the impact of TrO_3-Phot on ozone, process analysis of improved IPR is applied to quantify the contributions of different physical and chemical processes to O_3 concentrations, and their differences between BASE and $WoTrO_3Phot$ cases are detailed discussed. Fig. 7(d1-d4) show the changes in the contribution of each process caused by TrO_3-Phot over eastern China, NCP, YRD, and PRD. TrO_3-Phot enhances the positive contributions of VMIX (+155.1, +220.8, +218.3, +130.3 μg·m^{-3}), SGCV (+8.6, +11.9, +11.4, +16.5 μg·m^{-3}), and TRAN (+5.6, +42.3, +140.7, +125.2 μg·m^{-3}), while significantly intensifying chemical removal process (−170.2, −283.1, −375.3, −274.4 μg·m^{-3}), which ultimately dominates the reduction in O_3 concentrations.

Process analysis of integrated reaction rates (IRRs) for ozone-related and radical-related gas-phase chemical reactions is further analyzed to explain the negative feedback (i.e., TrO_3-Phot decreases near-surface ozone). As shown in Fig. 8, TrO_3-Phot enhances the reaction rates of O_3 with NOx (e.g., O_3 + NO and O_3 + NO_2), while suppressing the reactivity between HOx and NOx (e.g., OH + NO_2, HO_2 + NO_2, and HO_2 + NO). In other words, TrO_3-Phot reduces the concentration of HOx radicals, thereby weakening the HOx-related oxidation rates. As tropospheric O_3 can also function as an oxidant, it will become more actively engaged in oxidation reaction under these conditions, resulting in a negative net ozone production rate (Table 3), with values of −0.3, −0.3, −0.3, and − 0.2 ppbv h^{-1} for eastern China, NCP, YRD, and PRD, respectively, which can explain the overall decrease in O_3 concentrations.

5. Conclusions and limitations

Tropospheric ozone (O_3) is an important air pollutant and atmospheric oxidant. Meanwhile, it can also absorb shortwave and longwave radiation, and the changed radiation balance will cause a feedback impact on O_3 air quality. In this study, a fully coupled online WRF-Chem model is employed to investigate the impact of tropospheric ozone–radiation interactions, featuring a comprehensive integration of both meteorological feedback (TrO_3-Met) and photolysis feedback (TrO_3-Phot) effects on near-surface O_3 in June over eastern China. A ten-year simulation from 2010 to 2019 is conducted, and the multi-year averaged results can enhance the representativeness of quantified contributions of TrO_3-Met and TrO_3-Phot. Process analysis of the improved IPR (integrated process rate) and IRR (integrated reaction rate) is also applied to identify the dominant physical/chemical process for elucidating the underlying mechanism of increased/decreased near-surface O_3 due to the impacts of TrO_3-Met and TrO_3-Phot.

In general, the WRF-Chem model can well reproduce the spatio-temporal distribution of observed O_3 concentrations (including in-situ observations and satellite retrieved tropospheric column ozone) and meteorological parameters (including air temperature, relative humidity, and wind speed), with IOAs (index of agreement) of 0.59–0.93.

Sensitivity experiments show that TrO_3-Met increases the net radiative forcing at the tropopause, near-surface air temperature and PBLH by +3.4 W m^{-2}, +0.05 °C, and + 1.9 m averaged over eastern China, respectively. The altered radiation flux and meteorological variables further elevate surface-layer O_3 concentrations by +0.1 μg·m^{-3}, with more pronounced effects simulated over metropolitan regions, such as the North China Plain (NCP, +0.4 μg·m^{-3}), Yangtze River Delta (YRD, +0.5 μg·m^{-3}), and Pearl River Delta (PRD, +0.1 μg·m^{-3}). The improved IPR indicates that the weakened TRAN input and the enhanced GASC removal decrease O_3 concentration, whereas the altered SGCV and VMIX contribute to increased O_3 levels, with the VMIX process being the dominant factor driving the net surface O_3 increase.

As a radiation-active gas, tropospheric O_3 influences gas-phase photolysis rates by the optical depth of ozone molecular absorption. Consequently, TrO_3-Phot reduces daytime $J[O^1D]$ by 34.5%, and then lowers the concentration of OH radical—a key product of photochemical reactions—by 21.0% on average across eastern China, ultimately leading to a 1.0% reduction (-1.0 μg·m^{-3}) in surface O_3 concentrations, with more pronounced reductions over NCP (−7.8%, −8.0 μg·m^{-3}), YRD (−6.4%, −4.8 μg·m^{-3}), and PRD (−4.2%, −2.7 μg·m^{-3}). Improved IPR shows that TrO_3-Phot enhances the positive contributions of VMIX, SGCV, and TRAN, while significantly intensified chemical removal process drives the final reduction in surface O_3. Further analysis of O_3-related gas-phase chemical reaction rates based on IRR reveals that weakened HOx-driven oxidation leads to enhanced involvement of tropospheric O_3 in alternative oxidation processes, resulting in a negative net O_3 production rate, thereby explaining the decline in surface O_3 concentrations.

This study highlights the role of tropospheric O_3 as a radiation-absorptive and radiation-active gas, explicitly quantifying the feedback effects of TrO_3-Met and TrO_3-Phot on ozone air quality. The

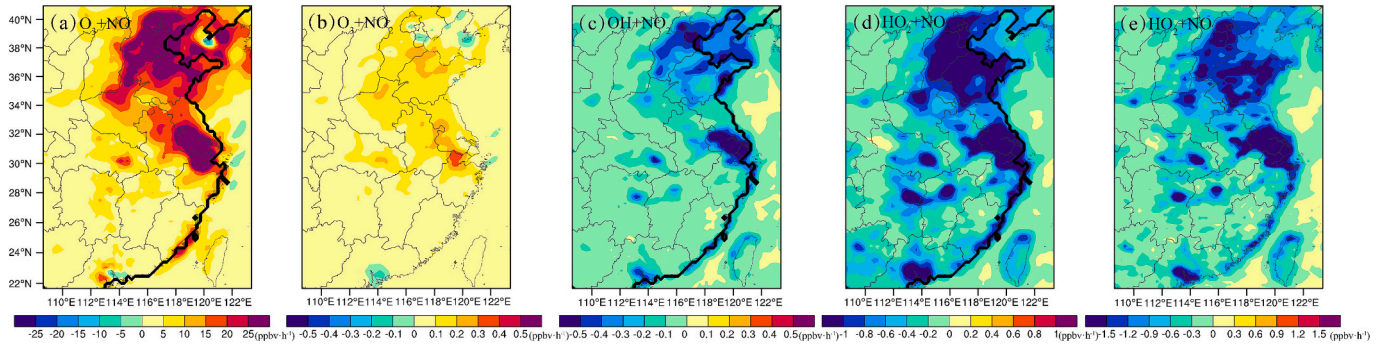

Fig. 8. Spatial distribution of the differences in simulated daytime (07:00–18:00 LST) chemical reaction rates of (a) O_3 + NO, (b) O_3 + NO_2, (c) OH + NO_2, (d) HO_2 + NO_2, and (e) HO_2 + NO between the cases of BASE and $WoTrO_3Phot$ (BASE minus $WoTrO_3Phot$) averaged in June during 2010–2019.

Table 3
Ozone-related gas-phase chemical reaction rates simulated by cases of BASE and WoTrO$_3$Phot and their differences (BASE minus WoTrO$_3$Phot) averaged over eastern China (EC), North China Plain (NCP), Yangtze River Delta (YRD), and Pearl River Delta (PRD). Positive (negative) values represent chemical generation (depletion) of ozone.

Reaction (ppbv·h^{-1})	EC			NCP			YRD			PRD		
	BASE	WoTrO$_3$Phot	Delta	BASE	WoTrO$_3$Phot	Delta	BASE	WoTrO$_3$Phot	Delta	BASE	WoTrO$_3$Phot	Delta
$O_3 + hv \rightarrow O(^3P) + O_2$	−3.2	−5.0	+1.8	−2.4	−4.6	+2.2	−3.0	−5.8	+2.8	−1.8	−2.9	+1.1
$O_3 + hv\_a \rightarrow O(^1D) + O_2$	−56.9	−58.2	+1.3	−54.7	−61.6	+6.9	−56.9	−62.0	+5.1	−26.6	−28.8	+2.2
$OH + O_3 \rightarrow HO_2 + O_2$	−0.08	−0.1	+0.02	−0.05	−0.09	+0.04	−0.07	−0.1	+0.03	−0.05	−0.07	+0.02
$HO_2 + O_3 \rightarrow OH + 2O_2$	−0.1	−0.1	0.0	−0.04	−0.08	+0.04	−0.06	−0.1	+0.04	−0.06	−0.09	+0.03
$O_3 + NO \rightarrow NO_2 + O_2$	−94.4	−85.8	−8.6	−317.0	−284.3	−32.7	−324.8	−296.3	−28.5	−182.7	−176.7	−6.0
$O_3 + NO_2 \rightarrow NO_3 + O_2$	−0.8	−0.7	−0.1	−2.1	−1.9	−0.2	−2.2	−2.0	−0.2	−1.5	−1.5	0.0
$O + M \rightarrow O_3 + M$	+150.1	+144.9	+5.2	+360.8	+337.3	+23.5	+363.4	+343.1	+20.3	+199.3	+196.9	+2.4
Net O_3 production rate	−5.4	−5.1	−0.3	−15.5	−15.2	−0.3	−23.6	−23.3	−0.3	−13.4	−13.2	−0.2

findings can contribute to a better understanding of the impacts of tropospheric ozone on weather and climate, and support the development of effective ozone pollution control strategies in China, and even other regions facing similar high tropospheric column ozone concentration.

There are also some limitations in this work. (1) The simulation performances of ozone concentrations and the impacts of TrO$_3$-Met and TrO$_3$-Phot can be influenced by different model configurations including physical and chemical parameterizations, emission inventories and other factors (Zhong et al., 2016; Weng et al., 2026). For example, Weng et al. (2023) selected two different chemical mechanisms of MOZART (Model for Ozone and Related Chemical Tracers) and CBMZ (Carbon Bond Mechanism Z) to predict changes in summertime ozone concentrations from 2017 to 2030 across China by using WRF-Chem. Their results show that CBMZ predicts ozone decreases of up to 12 ppb whereas MOZART projects an average increase of approximately 2 ppb. Therefore, in the future study we will quantitatively explore the extent of impacts of tropospheric ozone-radiation interactions on ozone over eastern China by using different model parameter settings, and conduct a deep analysis to explain the potential causes of the deviation. (2) We select June as the study period for quantifying the impacts of TrO$_3$-Met and TrO$_3$-Phot due to the high concentrations of both tropospheric column ozone (Fig. S3) and surface ozone (Fig. S4), and the frequent occurrence of ozone pollution (Liao et al., 2025; Wang et al., 2026). However, the impacts of tropospheric ozone-radiation interactions in other summer months (e.g., July) may differ from those in June. As shown in Fig. S5, the impact of TrO$_3$-Phot on surface ozone concentration in July 2019 is similar to that in June (Fig. S5(c)), while the TrO$_3$-Met effect in July 2019 differs significantly from that in June (Fig. S5 (a)), which can be attributed to significant monthly meteorological fluctuations (Wang et al., 2025). Therefore, we will extend our study to cover all summer months to comprehensively analyze the impacts of tropospheric ozone-radiation interactions in the future study.

CRediT authorship contribution statement

Yuqi Guan: Formal analysis, Investigation, Validation, Writing – original draft. **Jia Zhu:** Conceptualization, Funding acquisition, Methodology, Supervision, Writing – review & editing. **Xueqing Wang:** Writing – review & editing, Validation, Software, Resources. **Lei Chen:** Writing – review & editing, Software, Funding acquisition, Conceptualization. **Xipeng Jin:** Validation, Resources. **Xu Yue:** Validation, Resources. **Hong Liao:** Validation, Funding acquisition.

Declaration of competing interest

The authors declare that they have no known competing financial interests or personal relationships that could have appeared to influence the work reported in this paper.

Acknowledgements

This research was supported by National Natural Science Foundation of China (grant no. 42305121, 42293323, 42007195).

Appendix A. Supplementary data

Supplementary data to this article can be found online at https://doi.org/10.1016/j.atmosres.2026.108817.

Data availability

Data will be made available on request.

References

Brasseur, G.P., Hauglustaine, D.A., Walters, S., Rasch, P.J., Müller, J.F., Granier, C., Tie, X.X., 1998. MOZART, a global chemical transport model for ozone and related chemical tracers: 1. Model description. J. Geophys. Res. Atmos. 103, 28265–28289. https://doi.org/10.1029/98jd02397.

Chang, W., Liao, H., Wang, H., 2009. Climate responses to direct radiative forcing of anthropogenic aerosols, tropospheric ozone, and long-lived greenhouse gases in eastern China over 1951–2000. Adv. Atmos. Sci. 26, 748–762. https://doi.org/10.1007/s00376-009-9032-4.

Chen, L., Liao, H., Li, K., Zhu, J., Long, Z., Yue, X., Yang, Y., Zhang, M., 2023. Process-level quantification on opposite $PM_{2.5}$ changes during the COVID-19 lockdown over the North China plain. Environ. Sci. Technol. Lett. 10, 779–785. https://doi.org/10.1021/acs.estlett.3c00490.

Chuang, M.-T., Chou, C.C.-K., Lin, C.-Y., Lee, J.-H., Lin, W.-C., Li, M.-H., Chen, S.-W., Chang, S.-H., 2024. $PM_{2.5}$ episodes in northern Taiwan under southerly winds in late winter. Atmos. Res. 311, 107686. https://doi.org/10.1016/j.atmosres.2024.107686.

Cooper, O.R., Parrish, D., Ziemke, J., Balashov, N., Cupeiro, M., Galbally, I., Gilge, S., Horowitz, L., Jensen, N., Lamarque, J.-F., 2014. Global distribution and trends of tropospheric ozone: an observation-based review. Elementa 2, 000029. https://doi.org/10.12952/journal.elementa.000029.

Du, N., Chen, L., Liao, H., Zhu, J., Li, K., 2023. Impact of summer tropospheric ozone radiative forcing on meteorology and air quality in North China. Environ. Sci. 44, 3705–3714. https://doi.org/10.13227/j.hjkx.202208098.

Fast, J.D., Gustafson Jr., W.I., Easter, R.C., Zaveri, R.A., Barnard, J.C., Chapman, E.G., Grell, G.A., Peckham, S.E., 2006. Evolution of ozone, particulates, and aerosol direct radiative forcing in the vicinity of Houston using a fully coupled meteorology-chemistry-aerosol model. J. Geophys. Res. Atmos. 111. https://doi.org/10.1029/2005JD006721.

Feng, T., Zhao, S., Hu, B., Bei, N., Zhang, X., Wu, J., Li, X., Liu, L., Wang, R., Tie, X., 2021. Assessment of atmospheric oxidizing capacity over the Beijing-Tianjin-Hebei (BTH) area, China. J. Geophys. Res. Atmos. 126, e2020JD033834. https://doi.org/10.1029/2020JD033834.

Gao, Y., Zhang, M., Liu, Z., Wang, L., Wang, P., Xia, X., Tao, M., Zhu, L., 2015. Modeling the feedback between aerosol and meteorological variables in the atmospheric boundary layer during a severe fog–haze event over the North China Plain. Atmos. Chem. Phys. 15, 4279–4295. https://doi.org/10.5194/acp-15-4279-2015.

Gao, J., Li, Y., Zhu, B., Hu, B., Wang, L., Bao, F., 2020. What have we missed when studying the impact of aerosols on surface ozone via changing photolysis rates? Atmos. Chem. Phys. Discuss. 2020, 1–28. https://doi.org/10.5194/acp-20-10831-2020.

Grell, G.A., Peckham, S.E., Schmitz, R., McKeen, S.A., Frost, G., Skamarock, W.C., Eder, B., 2005. Fully coupled "online" chemistry within the WRF model. Atmos. Environ. 39, 6957–6975. https://doi.org/10.1016/j.atmosenv.2005.04.027.

Guenther, A., Karl, T., Harley, P., Wiedinmyer, C., Palmer, P.I., Geron, C., 2006. Estimates of global terrestrial isoprene emissions using MEGAN (model of emissions of gases and aerosols from nature). Atmos. Chem. Phys. 6, 3181–3210. https://doi.org/10.5194/acp-6-3181-2006.

He, S., Carmichael, G.R., 1999. Sensitivity of photolysis rates and ozone production in the troposphere to aerosol properties. J. Geophys. Res. Atmos. 104, 26307–26324. https://doi.org/10.1029/1999JD900789.

Iacono, M.J., Delamere, J.S., Mlawer, E.J., Shephard, M.W., Clough, S.A., Collins, W.D., 2008. Radiative forcing by long-lived greenhouse gases: calculations with the AER radiative transfer models. J. Geophys. Res. Atmos. 113. https://doi.org/10.1029/2008JD009944.

Jiménez, P.A., Dudhia, J., 2012. Improving the representation of resolved and unresolved topographic effects on surface wind in the WRF model. J. Appl. Meteorol. Climatol. 51, 300–316. https://doi.org/10.1175/JAMC-D-11-084.1.

Kitayama, K., Morino, Y., Yamaji, K., Chatani, S., 2019. Uncertainties in O_3 concentrations simulated by CMAQ over Japan using four chemical mechanisms. Atmos. Environ. 198, 448–462. https://doi.org/10.1016/j.atmosenv.2018.11.003.

Li, M., Zhang, Q., Kurokawa, J.-I., Woo, J.-H., He, K., Lu, Z., Ohara, T., Song, Y., Streets, D.G., Carmichael, G.R., 2017. MIX: a mosaic Asian anthropogenic emission inventory under the international collaboration framework of the MICS-Asia and HTAP. Atmos. Chem. Phys. 17, 935–963. https://doi.org/10.5194/acp-17-935-2017.

Li, S., Wang, T., Huang, X., Pu, X., Li, M., Chen, P., Yang, X.Q., Wang, M., 2018. Impact of East Asian summer monsoon on surface ozone pattern in China. J. Geophys. Res. Atmos. 123, 1401–1411. https://doi.org/10.1002/2017JD027190.

Li, Y., Wang, T., Wang, Q.G., Li, M., Qu, Y., Wu, H., Xie, M., 2025. Impact of aerosol-radiation interaction and heterogeneous chemistry on the winter decreasing $PM_{2.5}$ and increasing O_3 in Eastern China 2014–2020. J. Environ. Sci. 151, 469–483. https://doi.org/10.1016/j.jes.2024.04.010.

Liao, Z., Zhang, J., Gao, M., Ma, Z., 2025. Widespread stratospheric intrusion influence on summer ozone pollution over China revealed by multi-site ozonesonde and validated EAC4 reanalysis. Atmos. Chem. Phys. 25, 14865–14877. https://doi.org/10.5194/acp-25-14865-2025.

Lu, X., Hong, J., Zhang, L., Cooper, O.R., Schultz, M.G., Xu, X., Wang, T., Gao, M., Zhao, Y., Zhang, Y., 2018. Severe surface ozone pollution in China: a global perspective. Environ. Sci. Technol. Lett. 5, 487–494. https://doi.org/10.1021/acs.estlett.8b00366.

Madronich, S., Flocke, S., 1997. Theoretical estimation of biologically effective UV radiation at the Earth's surface. In: Solar Ultraviolet Radiation: Modelling, Measurements and Effects. Springer, pp. 23–48. https://doi.org/10.1007/978-3-662-03375-3_3.

Myhre, G., Shindell, D., Bréon, F.-M., Collins, W., Fuglestvedt, J., Huang, J., Koch, D., Lamarque, J.-F., Lee, D., Mendoza, B., 2014. Anthropogenic and natural radiative forcing. In: Climate Change 2013-The Physical Science Basis, pp. 659–740. https://doi.org/10.1017/CBO9781107415324.018.

Pierrehumbert, R.T., Brogniez, H., Roca, R., 2007. On the relative humidity of the atmosphere. The global circulation of the atmosphere 143, 185. https://doi.org/10.1515/9780691236919-008.

Qiao, W., Li, K., Yang, Z., Chen, L., Liao, H., 2024. Implications of the extremely hot summer of 2022 on urban ozone control in China. Atmos. Ocean. Sci. Lett. 17, 100470. https://doi.org/10.1016/j.aosl.2024.100470.

Qin, M., Hu, A., Mao, J., Li, X., Sheng, L., Sun, J., Li, J., Wang, X., Zhang, Y., Hu, J., 2022. $PM_{2.5}$ and O_3 relationships affected by the atmospheric oxidizing capacity in the Yangtze River Delta, China. Sci. Total Environ. 810, 152268. https://doi.org/10.1016/j.scitotenv.2021.152268.

Qiu, Y., Liao, H., Zhang, R., Hu, J., 2017. Simulated impacts of direct radiative effects of scattering and absorbing aerosols on surface layer aerosol concentrations in China during a heavily polluted event in February 2014. J. Geophys. Res. Atmos. 122, 5955–5975. https://doi.org/10.1002/2016JD026309.

Qu, Y., Voulgarakis, A., Wang, T., Kasoar, M., Wells, C., Yuan, C., Varma, S., Mansfield, L., 2020. A study of the effect of aerosols on surface ozone through meteorology feedbacks over China. Atmos. Chem. Phys. Discuss. 2020, 1–26. https://doi.org/10.5194/acp-21-5705-2021.

Shindell, D., Faluvegi, G., Lacis, A., Hansen, J., Ruedy, R., Aguilar, E., 2006. Role of tropospheric ozone increases in 20th-century climate change. J. Geophys. Res. Atmos. 111. https://doi.org/10.1029/2005JD006348.

Sillman, S., 1999. The relation between ozone, NOx and hydrocarbons in urban and polluted rural environments. Atmos. Environ. 33, 1821–1845. https://doi.org/10.1016/S1352-2310(98)00345-8.

Taha, H., Sailor, D., 2010. Evaluating the effects of radiative forcing feedback in modelling urban ozone air quality in Portland, Oregon: two-way coupled MM5–CMAQ numerical model simulations. Bound.-Layer Meteorol. 137, 291–305. https://doi.org/10.1007/s10546-010-9533-9.

Wang, J., Allen, D.J., Pickering, K.E., Li, Z., He, H., 2016. Impact of aerosol direct effect on East Asian air quality during the EAST-AIRE campaign. J. Geophys. Res. Atmos. 121, 6534–6554. https://doi.org/10.1002/2016JD025108.

Wang, T., Xue, L., Brimblecombe, P., Lam, Y.F., Li, L., Zhang, L., 2017. Ozone pollution in China: a review of concentrations, meteorological influences, chemical precursors, and effects. Sci. Total Environ. 575, 1582–1596. https://doi.org/10.1016/j.scitotenv.2016.10.081.

Wang, X., Zhu, J., Jiao, G., Chen, X., Yang, Z., Chen, L., Jin, X., Liao, H., 2025. Meteorological influence on surface ozone trends in China: assessing uncertainties caused by multi-dataset and multi-method. Atmos. Chem. Phys. 25, 13863–13878. https://doi.org/10.5194/acp-25-13863-2025.

Wang, F., An, X., Sheng, L., 2026. Extreme ozone pollution over North China linked to rossby waves induced by North Atlantic sea surface temperature. Atmos. Res. 331, 108668. https://doi.org/10.1016/j.atmosres.2025.108668.

Weng, X., Li, J., Forster, G.L., Nowack, P., 2023. Large modeling uncertainty in projecting decadal surface ozone changes over city clusters of China. Geophys. Res. Lett. 50, e2023GL103241. https://doi.org/10.1029/2023GL103241.

Weng, X., Li, J., Zeng, G., Lu, X., Forster, G., Nowack, P., 2026. Divergent ozone predictions in China under carbon neutrality: why chemical mechanisms disagree. Environ. Sci. Technol. https://doi.org/10.1021/acs.est.5c10697.

Wiedinmyer, C., Akagi, S., Yokelson, R.J., Emmons, L., Al-Saadi, J., Orlando, J., Soja, A., 2011. The fire inventory from NCAR (FINN): a high resolution global model to estimate the emissions from open burning. Geosci. Model Dev. 4, 625–641. https://doi.org/10.5194/gmd-4-625-2011.

Xie, B., Zhang, H., Wang, Z., Zhao, S., Fu, Q., 2016. A modeling study of effective radiative forcing and climate response due to tropospheric ozone. Adv. Atmos. Sci. 33, 819–828. https://doi.org/10.1007/s00376-016-5193-0.

Xing, J., Wang, J., Mathur, R., Wang, S., Sarwar, G., Pleim, J., Hogrefe, C., Zhang, Y., Jiang, J., Wong, D.C., 2017. Impacts of aerosol direct effects on tropospheric ozone through changes in atmospheric dynamics and photolysis rates. Atmos. Chem. Phys. 17, 9869–9883. https://doi.org/10.5194/acp-17-9869-2017.

Yang, H., Chen, L., Liao, H., Zhu, J., Wang, W., Li, X., 2021. Impacts of aerosol-photolysis interaction and aerosol-radiation feedback on surface-layer ozone in North China during a multi-pollutant air pollution episode. Atmos. Chem. Phys. Discuss. 2021, 1–31. https://doi.org/10.5194/acp-22-4101-2022.

Yang, J., Wang, C., Zhang, Y., Zhang, S., Peng, X., Qin, X., Bai, J., Xue, L., Wang, G., Cui, S., 2025. Unprecedented impacts of meteorological and photolysis rates on ozone pollution in a coastal megacity of northern China. Atmos. Pollut. Res. 16, 102461. https://doi.org/10.1016/j.apr.2025.102461.

Zaveri, R.A., Easter, R.C., Fast, J.D., Peters, L.K., 2008. Model for simulating aerosol interactions and chemistry (MOSAIC). J. Geophys. Res. Atmos. 113. https://doi.org/10.1029/2007JD008782.

Zhang, Y., Lei, L., Ma, J., Wu, Q., Shu, Z., Feng, X., Wang, J., Jiang, T., 2024. Implications of ozone transport on air quality in the Sichuan Basin, China. Environ. Sci. Pollut. Res. 31, 43835–43851. https://doi.org/10.1007/s11356-024-33991-7.

Zhong, M., Saikawa, E., Liu, Y., Naik, V., Horowitz, L.W., Takigawa, M., Zhao, Y., Lin, N.-H., Stone, E.A., 2016. Air quality modeling with WRF-Chem v3.5 in East Asia: sensitivity to emissions and evaluation of simulated air quality. Geosci. Model Dev. 9, 1201–1218. https://doi.org/10.5194/gmd-9-1201-2016.

Zhou., 2010. Numerical Simulation Study on the Impact of Tropospheric Ozone in East Asia on Summer Temperature. Nanjing University of Information Science and Technology.